Estuaries and Coasts (2019) 42:1761–1773
https://doi.org/10.1007/s12237-019-00573-7

SPECIAL ISSUE: INTEGRATING ECOSYSTEMS AND COASTAL ENGINEERING PRACTICE

Short-Term Shoreline Trend Detection Patterns Using SPOT-5 Image Fusion in the Northwest of Yucatan, Mexico

Ana Patricia Ruiz-Beltran[1] · Alejandro Astorga-Moar[2] · Paulo Salles[1,2] · Christian M. Appendini[1,2]

Received: 13 July 2018 / Revised: 20 December 2018 / Accepted: 25 April 2019 / Published online: 29 May 2019

Abstract

Shoreline change is an important morphological feature used to identify impacts on coastal processes caused by coastal infrastructure or natural conditions (e.g., storms or sea level rise), providing insightful information for coastal and shoreline management. While shoreline measurements are not always available, remote sensing data can provide shoreline position in scarce data areas, as well as in large and inaccessible regions. Nevertheless, few studies have used multi-temporal remote sensing data to study gradual changes for time frames of less than 10 years due to the low spatial resolution for detecting small changes. In this study, we explore the use of image data fusion from the *Satellite Pour l'Observation de la Terre* - 5 (SPOT-5), taking into account the accuracy of shoreline mapping to detect changes in both disturbed and undisturbed coasts during 10 years in the northwestern Yucatan coast. Our results show that using image data fusion in SPOT-5 images is a feasible method to detect shoreline change trends in a relatively short time frame. Based on the proposed method, we were able to identify the factors leading to shoreline trends. This methodology proves useful for shoreline management and is appropriate for the planning of future developments in areas for which data are scarce.

Keywords SPOT-5 · Pan-sharpening · Shoreline change · DSAS · Spatial analysis · Coastal hazard · And human impacts

Introduction

Shorelines are dynamic systems that fluctuate over different time and spatial scales according to forcing agents and their interactions with coastal features (Boak and Turner 2005). Agents shaping the coast include a broad range of physical phenomena that arise from both natural processes and human intervention, resulting in changes in sediment flux (Silva-Casarín et al. 2014). In sandy coasts, the sediment budget represents the balance between sand input and output within a system. Shifts in sediment budget are an environmental indicator of alterations on coastal processes, usually as a result of a reduction or increase of sediment sources to the littoral cell, as well as shifts in wave climate and hydrodynamics. For instance, shoreline erosion can indicate a decrease of sand input into the system as a result of sand retention by dams (Syvitski and Milliman 2017) or updrift coastal structures, whereas beach widening might be a result of beach nourishment. As such, changes in shoreline position reflect changes in forcing agents as well as human interventions, both modifying sediment transport patterns within the littoral cell as a result of sand redistribution within the system.

Increasing anthropogenic pressure (e.g., sand retention by dams and mining, and modification of transport patterns by coastal infrastructure) directly modifies the sediment budgets and sediment transport patterns (Defeo et al. 2009) and can result in shoreline position fluctuations. Besides the anthropogenic factors, natural factors such as sea level rise and storms are expected to vary with climate change. For instance, tropical cyclones are expected to increase in intensity (Knutson et al. 2010; Emanuel 2013; Kang and Elsner 2015), which will further escalate the stress on coastal regions and their ecosystem services (Day et al. 2008). Together with coastal encroachment leading to coastal squeeze (Pontee 2013), exacerbated erosional processes have myriad negative consequences, including impacting the population of turtles and coastal birds due to habitat reduction, increasing the

Communicated by Mead Allison

✉ Ana Patricia Ruiz-Beltran
a.ruizbeltran@uq.edu.au

✉ Christian M. Appendini
cappendinia@iingen.unam.mx

[1] Laboratorio Nacional de Resiliencia Costera, Puerto de Abrigo s/n, 97356 Sisal, Yucatán, Mexico

[2] Laboratorio de Ingeniería y Procesos Costeros, Instituto de Ingeniería, Universidad Nacional Autónoma de México, Puerto de Abrigo s/n, 97356 Sisal, Yucatán, Mexico

vulnerability of coastal infrastructure and populations and making beaches less attractive for tourism.

As shoreline changes provide insight into the littoral processes and their interference with anthropogenic activities and infrastructure, they can be used to assess the effect of interventions in the past and help predict the impacts of interventions in the future. Furthermore, they can be useful together with other beach features (e.g., dune height and position, beach profile) to evaluate the long-term beach resilience (Houser et al. 2015). Considering that it is possible to obtain and analyze shoreline position on a spatially explicit context and over long periods (Gens 2010), shoreline mapping and change detection are critical for sustainable resource management and environmental protection (Di et al. 2003; Li and Damen 2010; Zulkifle et al. 2017). In situ measurements, such as beach profiles and water level measurements allow for accurate shoreline change detection; however, most areas of the world lack monitoring and mapping programs and are reliant upon available data. An alternative for studying inaccessible areas that lack field data is the use of satellite imagery. Satellite images provide historical information and cover vast areas, including those that are difficult to access. For this reason, satellite imagery has been commonly used for shoreline mapping at variable spatial scales over long periods.

Satellite shoreline mapping can be performed by using a single satellite sensor (Kuleli et al. 2011; W. Li and Gong 2016; Pardo-Pascual et al. 2012; Sagar et al. 2017) or the combination of multiple sensors with or without aerial images (Maiti and Bhattacharya 2009; Li and Damen 2010; Ford 2013; Castelle et al. 2018). However, the coarse spatial resolution often obtained via satellite imagery can make it difficult to detect subtle changes over short periods. Nevertheless, if a satellite has panchromatic and multi-spectral bands, the use of an image fusion algorithm between these bands can enhance both spatial resolution and visual quality (Zulkifle et al. 2017). Image fusion, also known as pan-sharpening, is the process in which two or more images are combined to produce an individual image that integrates the information of the combined images, effectively increasing their spatial and spectral resolutions (Pradham et al. 2011). Successful application of this technique has been demonstrated to increase classification accuracy (Lin et al. 2015) and reduce errors associated with change detection (Du et al. 2013). Image fusion methods have been applied to shoreline mapping studies (Pohl and Van Genderen 1998; Pranzini 2007; Li et al. 2008; Yang 2009; Maglione et al. 2014) but, to the best of our knowledge, have not been used to identify dynamic shoreline trends.

In this study, we analyze multi-temporal satellite imagery of the northwestern Yucatan coast using multi-temporal image fusion to enhance the spatial resolution from the *Satellite Pour l'Observation de la Terre - 5* (SPOT-5) imagery and allow coastal pattern detection. As with many anthropomorphized coastlines, the Yucatan coast contains erosional areas associated with non-engineered coastal protection structures and sediment transport gradients (Appendini et al. 2012; Lira-Pantoja et al. 2012). Comparing pristine and affected areas enables us to determine and understand the impacts of coastal structures on shoreline change. As such, the study aims to provide a method to characterize the medium-term (10-year) shoreline dynamic based on image fusion from SPOT-5, allowing detection and comparison of shoreline trends in pristine and human-affected beaches. This method allows for the extraction of fundamental information for coastal and shoreline managers, particularly for non-accessible areas or locations lacking monitoring programs.

Study Area

The study area is located on the northwestern coast of the Yucatan peninsula (Fig. 1), extending for approximately 50 km from the State Reserve El Palmar (21° 2′ 10.71″ N, 90° 17′ 52.05″ W) to the western side of Chuburna harbor jetties (21° 14′ 49.05″ N., 89° 50′ 43.98″ W). The shoreline under study comprises the following zones: (1) the natural protected area (State Reserve El Palmar) which is considered "pristine", reflecting an area with no human infrastructure despite the fact that shoreline processes could be influenced by human interventions in other areas of the littoral cell; (2) the developed shoreline along the town of Sisal, where fishing and recreational beach activities take place and where there is a harbor with jetties and the old Sisal dock, both affecting sediment transport; (3) the natural area between Sisal and Chuburna, which is a pristine area similar to El Palmar; and (4) the area west of the Chuburna jetties, which is a natural area generally devoid of human activity, but severely affected by erosion due to the effect of the jetties on sediment transport. The morphological changes at the inlet of the coastal lagoon La Carbonera (located between zones 3 and 4) involve complex processes beyond the scope of this study resulting in the exclusion of this area from our analysis.

The study area is characterized as a barrier island system with a 1/1000 slope wide continental shelf (Herrera-Silveira et al. 2010), with a mixed micro-tidal regime with diurnal dominance. Sediment sources are mainly biogenic as there are no rivers in Yucatan, and the sediment is mainly composed of skeletal fragments (Neal et al. 2016). Sediment transport is mainly driven by NE waves arriving the coast with a mean significant wave height of 0.75 m and periods of 5 s at 20 m depth, generating a dominant net sediment transport towards the west (Appendini et al. 2012). However, during winter, the sediment transport is inverted during the arrival of NW waves generated by cold surge intrusions (*Nortes*) into the Gulf of Mexico (Appendini et al. 2018), which are more energetic (1–2.5 m waves with periods between 5 and 10 s at 10 m depth) but with a low occurrence (Appendini et al. *2012*).

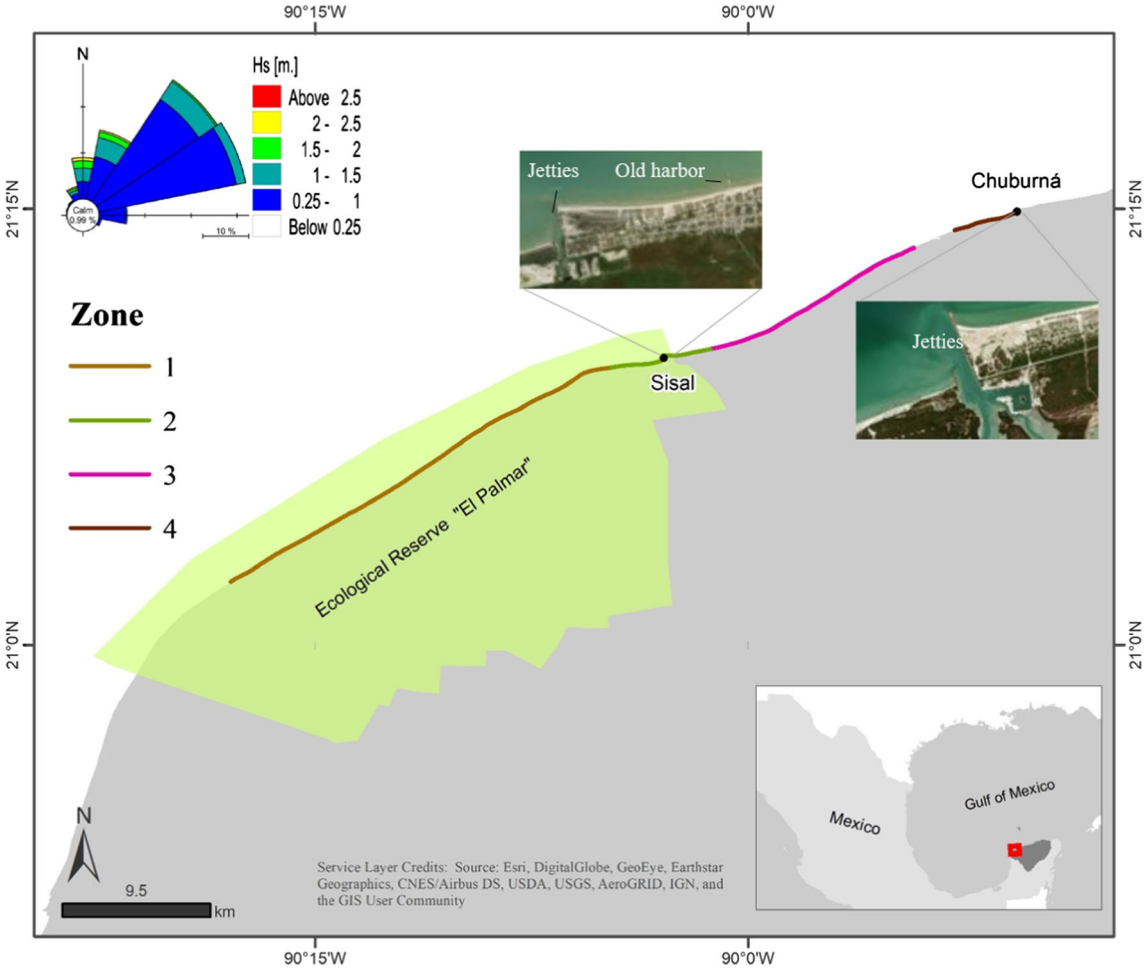

Fig. 1 The study area is represented by a line on the map, where different colors indicate each zone. The area is overlapped with at least six of the eight SPOT images. The western zone is located inside an ecological reserve. The wave rose indicates the wave climate in the area

Coastal research in Yucatan has addressed vulnerability to erosion and flooding (Mendoza et al. 2014; Cuevas Jiménez et al. 2016), beach morphodynamics (Cuevas-Jiménez and Euán-Ávila 2009; Ruiz-Martínez et al. 2015), and sediment transport (Appendini et al. 2012; Lira-Pantoja et al. 2012). Regarding shoreline change assessment studies, Cuevas-Jiménez and Euán-Ávila (2009) used in situ measurements over limited spatial scales, while García-Rubio et al. (2015) used a limited number of images to assess shoreline change over long periods. Both studies only considered the central portion of the Yucatan peninsula, where most of the touristic activities and residential development occur.

Methodology

To address the shoreline changes in the northwest coast of the Yucatan peninsula over a decade, we used eight multi-spectral and panchromatic satellite images from the SPOT-5 platform between 2004 and 2014, coupled with Digital Shoreline Analysis (DSAS). SPOT-5 images have four multi-spectral bands with a spatial resolution of 10 m in the green (500–590 nm), red (610–680 nm), near infrared (NIR, 780–890 nm), and short wavelength infrared (SWIR, 1580–1750 nm), while it has one panchromatic band (480–710 nm) with a spatial resolution of 2.5 m. These images are suitable for shoreline extraction as SPOT-5 includes two of the spectral bands that are the most effective for the visualization of the shoreline with the combination of MIR, NIR, and green bands (Li and Damen 2010; Petropoulos et al. 2015). The images were obtained during different times of the year and at different astronomical tide heights (Table 1). The astronomical tide heights were determined using the tidal constituents from analyzing the measured water levels in Sisal, Yucatan, located in the study area. Nevertheless, we did not consider the tidal height, which due to the SPOT-5 spatial resolution leads to an error between 1 and 2 pixels as the shoreline position varies between 2.5 and 4 m when considering the minimum and maximum astronomical tides (Espadas-Sánchez 2017). Such an error is indeed considered when determining shoreline trends. An overview of the methodology is shown in Fig. 2.

Table 1 Date of acquisition of multi-spectral and panchromatic SPOT-5 images and their corresponding astronomical tide level

Year	Month	Day	Tide (mm)
2004	March	10	50
2006(a)	January	15	− 360
2006(b)	November	28	− 90
2007	April	08	270
2009	January	01	− 390
2011	January	04	− 310
2012	March	21	− 60
2014	March	03	− 60

Pan-Sharpening Assessment

When applying an image fusion algorithm between high spatial resolution panchromatic and low spatial resolution multi-spectral data, it is important to maintain the spectral fidelity as much as possible to the resulting image fusion (Garguet-Duport et al. 1996; Ashraf et al. 2012). As such, the selection of an appropriate fusion method is essential for improving image analysis accuracy (Bai et al. 2015). For selecting the most accurate image fusion algorithm, we used the correlation coefficient, which is considered to be a spectral quality metric to test pan-sharpening (Vijayaraj 2004; Pradham et al. 2011). Two image fusion algorithms were tested by checking the correlation of pixels between unsharpened and pan-sharpened pairs of bands. The tested algorithms corresponded to the category of multi-resolution-based pan-sharpening, as we needed to increase the spectral and spatial resolution of all our bands. These algorithms were subtractive resolution merge (SRM) and hyperspherical color space resolution merge (HCS). The rest of the methods available in ERDAS Imagine were excluded from the analysis because they considered only three bands, or the ratio between the panchromatic and multi-spectral band was not ideal for our images. The SRM algorithm was tested over other algorithms on a similar environment, i.e., freshwater coastal areas (Ashraf et al. 2012), while the HCS algorithm produced a fused image with acceptable color and spatial recovery (Padwick et al. 2010). HSC is a method designed to be used with the WorldView 2 satellite, which presents a spatial resolution of 0.64 and 1.84 m in its panchromatic and multi-spectral bands, which is the same ratio between the multi-spectral and panchromatic SPOT-5 bands.

To assess the image fusion methods, we selected a subset of 1975 × 5615 pixels in a highly heterogeneous land cover, including sand, human settlements, lagoons, mangroves, and dune vegetation (Fig. 3). The pixels from the original multi-spectral bands were divided into 16 pixels for comparison with the fused images. To conserve the natural shoreline shape, we used the cubic convolution resampling method (Alparone et al. 2015). After finding the image fusion algorithm best suited to our study, it was applied to the rest of the images.

The resulting pan-sharpened images were co-registered to the 2014 image, ensuring a root mean square error (RMSE) < 0.5 pixels. Image co-registration is a pre-requisite for change detection to geometrically align two images and to ensure that the corresponding pixels represent the same objects in reality (Huhdanpaa et al. 2014). The image pre-processing was performed using ERDAS Imagine 2015, which is a remote sensing software that supplies tools for geodata analysis.

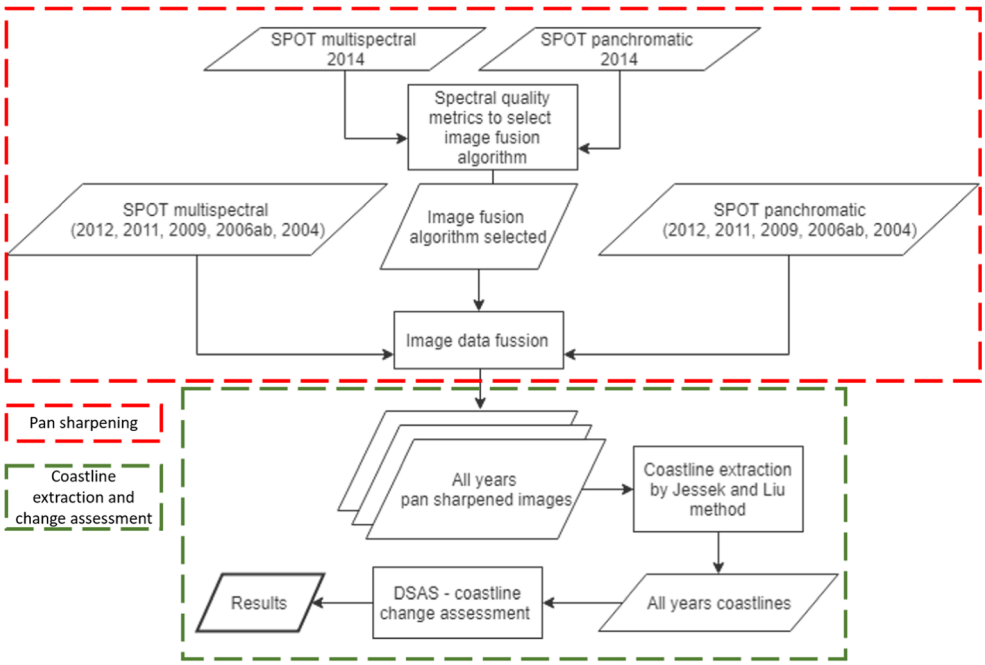

Fig. 2 Methodology flowchart

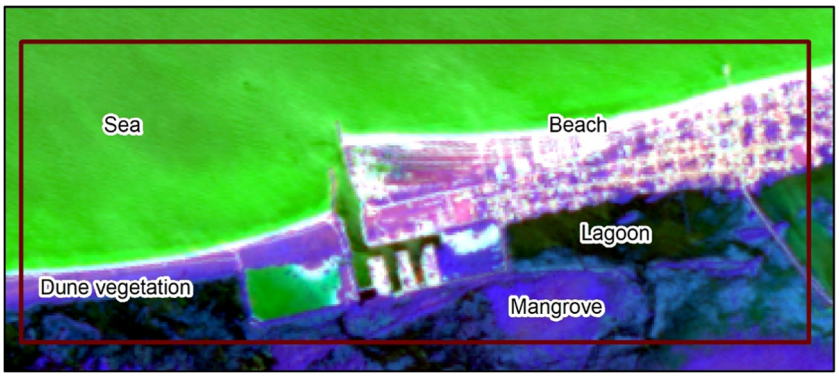

Fig. 3 Image fusion assessment subset denoted inside the purple box

Shoreline Extraction and Change Assessment

In this study, we understand shoreline as the water/landline, while coastline as the line of a more permanent morphological structure such as the toe of bluffs or cliffs, dunes, or vegetation lines. To characterize the morphological changes on the shoreline, we then used the instantaneous water line to define the shoreline position at both the pristine and human-affected areas. We used this definition of shoreline as it is a good indicator in micro-tidal and low slope beaches (Sytnik et al. 2018) which are typical of the northern coast of the Yucatan Peninsula.

The shorelines were extracted from the satellite images using the method proposed by Liu and Jezek (2004). This method consists of three groups of image processing algorithms: pre-segmentation, segmentation, and post-segmentation. In the pre-segmentation stage, two filters are applied to all the images (noise reduction and edge enhancement), allowing the shoreline to show a higher contrast with the other land covers in the image. The SWIR band (1.580–1.750 μm) exhibits a sharp contrast between land and water features due to the high degree of absorption by water and the strong reflectance by vegetation and natural features in the range. Thus, the MNDWI algorithm, which is a combination of green and mid-infrared bands, is ideal for discriminating between land and water at their interface (Ghosh et al. 2015). However, when using the method of Liu and Jezek (2004), which only accepts one band, the green band was selected since it presented a better overall performance in exhibiting a higher contrast between the sand and the water than the SWIR band (Fig. 4). The exceptions were the images for 2006b and 2011, where the tide level was − 36 cm and − 33 cm, respectively. For those tidal levels, the exposed sandbars appeared to have the same pixel values as the beach in the green band, preventing the precise extraction of the shoreline position (Fig. 5). Therefore, we used the SWIR band (Fig. 5c) for these images, considering this band is better suited for low tide conditions. During the segmentation stage, the images were partitioned into squares of 25 × 25 pixels to select only two types of land cover: water and sand. As the beach in the coast of Yucatan is relatively narrow, the frequency of the water cover was higher in each square to avoid the presence of the vegetation class, which had similar values as the water. We, therefore, forced the samples to have only these two classes, and we avoided the bimodality test mentioned by Liu and Jezek (2004). Finally, during the post-segmentation stage, we extracted the coastal edges by first producing a binary image output (water and sand) and then by delineating the shoreline between the edges of these two land cover types. The precision of the shoreline is measured at the spatial resolution of the fused images, which in this case is 2.5 m. We then used Matlab scripts to identify the shoreline on the satellite images following the methodology of Liu and Jezek (2004). We did not consider the few areas where the shoreline could not be extracted due to the presence of clouds and/or macroalgae. However, if a cloud shadow covered the shoreline, we corrected the line manually as it was visible, but it was not possible to be extracted with the Jesek and Liu method. We finally calculated each shoreline error as the sum of the error of the image co-registration plus the pixel size error for the method to extract the shorelines.

To assess the possible type of shoreline changes over our study timeframe and the data employed, we used the Digital Shoreline Analysis System (DSAS) Version 4.0 developed by Thieler et al. (2009). DSAS is a software extension for ArcGIS developed by the US Geological Survey widely used to assess shoreline changes. This program plots transects perpendicular to a baseline and calculates the distance from the baseline to the shoreline for each transect on each image. In our study, we plotted transects separated at 50 m intervals with a longitude of 350 m. We created the baseline with a 50-m buffer of the 2014 shoreline and smoothed it manually to obtain a straight line. Measurements were computed only if there were at least five shorelines in the same transect, resulting in 960 transects in our study area. The measures used to assess the shoreline change were the shoreline change envelop (SCE), weighted linear regression (WLR), and net shoreline movement (NSM) with a 95% confidence interval. SCE is the distance in meters

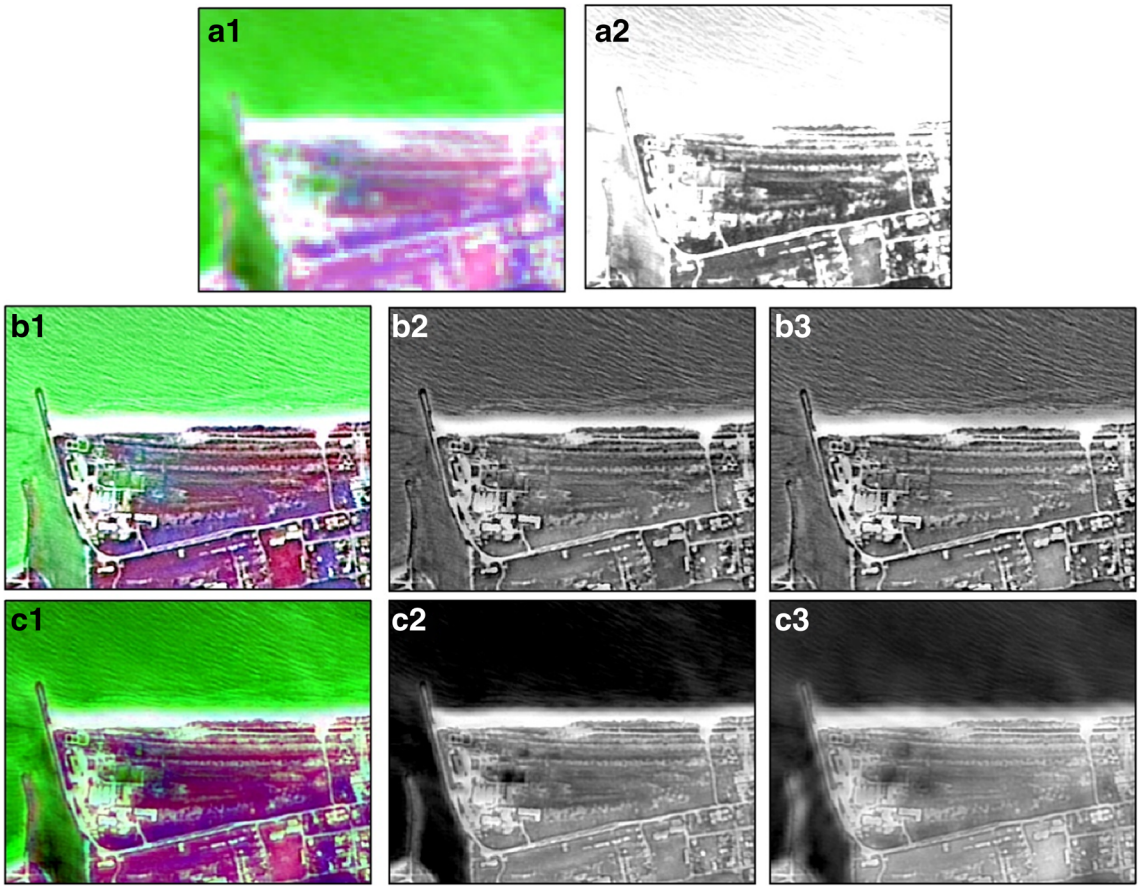

Fig. 4 Original and fused images. a1 and a2 are the original multispectral and panchromatic images. The b images corresponds to the images fused with SRM, where b2 is the green band and b3 the SWIR. The c images are the images fused with HCS where c2 corresponds to the green band and c3 to SWIR. The RGB combination for the false color (a1, 1, and c1) is SWIR, NIR, and green

between the closest and farthest shorelines to the baseline and therefore represents the variability of the shoreline between the years. Weighted Linear Regression (WRL) is the trend of change in meters per year taking into account the shoreline position error. Within our spatial resolution, we classified four types of shorelines: erosional, accretion, dynamic, and stable. The transects with either positive or negative WRL and with an r^2 value higher than a specific threshold were considered erosional or accretional shorelines. The threshold value was obtained by comparing r^2 with the absolute value of SCE/NSM and identifying the r^2 where the SCE/NSM ceases to fluctuate and remains near one. We determined a minimum r^2 value of 0.68 as the threshold to identify shorelines with erosional or accretional trends (Fig. 6).

The remaining transects were assessed by SCE and were consider either stable or dynamic shorelines based on the shoreline errors and therefore the limits of the mapping accuracy. Since we use a minimum of five shorelines to compute the SCE, stable shorelines were considered to have a change in position that is five times less than the maximum shoreline error, while dynamic shorelines were considered to have an SCE higher than five times the maximum shoreline error.

Results

Pan-Sharpening Assessment

We compared the HSC and the SRM pan-sharpening methods on SPOT-5 images, which helped delineate the shoreline with higher precision than only using the multispectral bands. In most of the original panchromatic images, the shoreline was not visible as it presented a saturation in the area of water and land, while the pan-sharpening method allowed us to discern the shoreline (Fig. 4). While the visual interpretation showed more enhancement with the SRM method (Fig. 4b1) in the green (Fig. 4b2) and the SWIR bands (Fig. 4b3), the HCS showed a better contrast between land and water, enhancing the shoreline visualization (Fig. 4c2 and 4c3). Furthermore, the HCS was the method with the higher inter-correlation between each pair of the unsharpened bands and the sharpened band, with r^2 values greater than 0.9 ($p > 0.05$), while the SMR presented r^2 values around 0.7 (Table 2). As a result, we used the HCS method for image fusion in the remaining images.

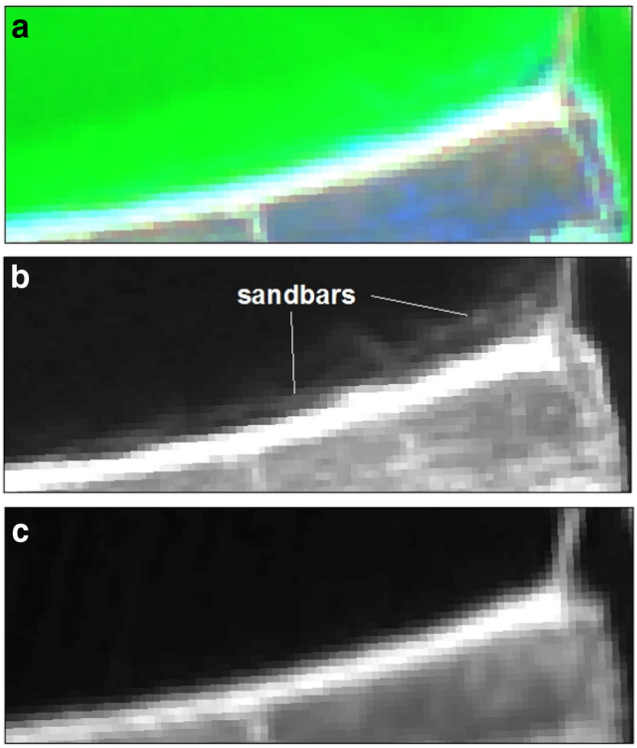

Fig. 5 Four hundred and twenty-one false color (**a**), green (**b**) and SWIR (**c**) for the 2011 image. Sandbars are noted in the green band (**b**), while in the SWIR, these are not visible (**c**). The same effect is presented with the 2006b image during low tide

Shoreline Extraction and Change Assessment

Errors of the shorelines relative to the reference shoreline position varied from 2.5 to 3.75 m (Table 3). The minimum error corresponded to the image of 2014 as it was the reference for co-registering the rest of the images, and therefore, it did not include the co-register error. We used these values to compute the measurements for WLR and r^2 in the DSAS analysis.

We assume that the value of $r^2 > 0.68$ indicates that shoreline changes over the year had a significant trend, and therefore, tidal variations did not interfere in detecting these patterns (Fig. 7). As observed in Fig. 7b, there is a clear tendency of erosion as the shoreline in 2004 is followed by a retreated shoreline in 2006a and sequentially until the most retreated position in 2014. Other areas also present a relatively high value of WLR; however, we cannot infer if these areas have a pattern of erosion or accretion because of the low r^2 value (Fig. 7c), and therefore, coastal processes in these transects produce a more dynamic shoreline. In other areas, the shoreline errors overlapped between each other, and we consider them as stable areas within the 10-year timeframe of our study (Fig. 7d).

A total of 960 transects were analyzed to detect shoreline patterns in the northwest of the Yucatan Peninsula. Changes range from − 6.45 to 5.63 m/year for WLR and from 3.88 to 67.3 m for SCE. All the zones presented an average negative WLR value, with an average SCE above 24 m. The effect of the Chuburna jetties blocking the longshore sediment transport from reaching zone 4 was evident as the average WLR was − 3.7 m/year (Table 4) with 67% of the transects showing an erosional trend and 31% classified as dynamic. Another area affected by jetties was zone 2, showing most of the erosion downstream of the jetties and accretion upstream (Fig. 8). Interestingly, the transects immediately downstream of the jetties in zones 4 and 2 were dynamic, which could be a result of sediment transport inversion during *Norte* events creating an accumulation of sand in these areas, accumulation due to transport inversion as a result of the jetties diffraction, and/or the result of human intervention. Zone 1 is characterized by erosion (average WLR of − 3.6 + − 1.3 m/year) and accretion (average WLR of 2.92 + − 1.0 m/year) areas alternated with dynamic stretches. In contrast to zone 1, 65% of the transects in zone 3 were dynamic, while 31% were stable. After the immediate accumulation of sand downdrift of the jetties, both

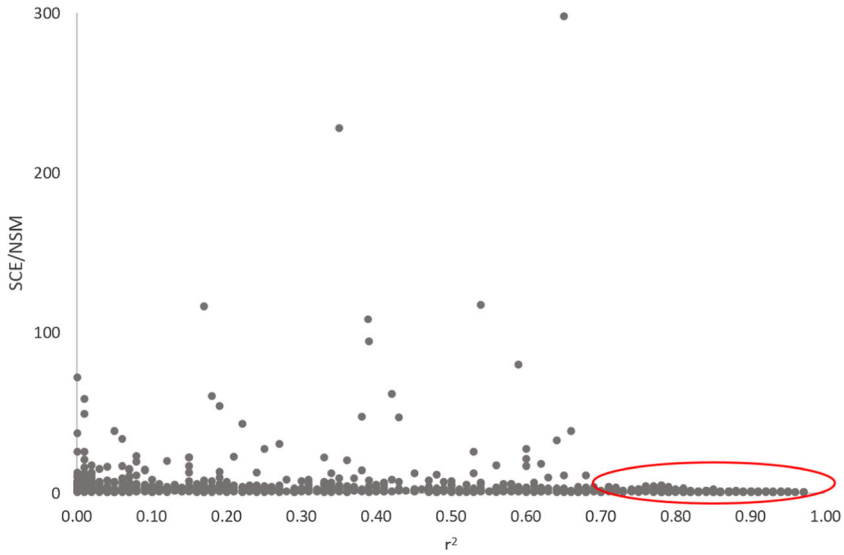

Fig. 6 SCE/NSM absolute values vs. r^2. The constant values of erosion and accretion are indicated in the red circle. The threshold value of r^2 is 0.68

Table 2 Inter-correlation parameters ($p > 0.05$) between the original bands and the fused bands with different pan-sharpening methods

Regression coefficient	HCS Band				SRM Band			
	Green	Red	NIR	SWIR	Green	Red	NIR	SWIR
r	*0.964*	*0.945*	*0.956*	*0.972*	0.675	0.706	0.724	0.665
b	− 0.478	1.302	1.000	− 0.519	36.089	44.585	40.648	32.446
m	1.000	0.981	0.986	1.000	0.540	0.689	0.816	0.472
RSME	0.000	0.000	0.000	0.000	0.000	0.000	0.000	0.000

zones 1 and 3 show erosion up to 2.5 and 3.3 km downdrift of the jetties respectively, with minimum erosion of − 1.72 and maximum of − 5.34 m/year.

Discussion

Pan-Sharpening Assessment

The HCS pan-sharpening method outperformed the SRM in our analysis, but other studies should consider analyzing different algorithms to select the most appropriate for their specific area. For instance, Wang et al. (2018) compared different methods, finding that for Landsat-Oli, the Brovey Transform method performed better, while Ashraf et al. (2012) found that SRM performed better when using Quickbird. Other works have also used different pan-sharpening algorithms to extract the shoreline from satellite images (Pranzini 2007; Alhin and Niemeyer 2009; Maglione et al. 2014). Considering that the performance of the pan-sharpening algorithm used varies depending on both satellite and environmental conditions, we recommend that shoreline studies provide a comparative assessment of the available pan-sharpening methods regardless of the remote-sensing software package.

We calculated the shoreline error by summing the positional error (2.5 m) + co-registering error. Although other people have used more precise methods to estimate the shoreline (Kermani et al. 2016; Li and Gong 2016), we did not have enough data to perform such calculations, which will be the case for most of the coastlines of the world or studies at a regional scale. Our maximum shoreline error was 3.725 m, which would have resulted in an error of at least 10 m without performing image fusion, as this is the pixel size of the multispectral images of SPOT-5. We would therefore not be able to identify shoreline patterns and differentiate between erosion, accretion, and dynamic shorelines as performed herein. Furthermore, we did not consider the tide, which has a variation between the minimum and maximum height from 2.4 to 4 m or 1–2 pixels (Espadas-Sánchez 2017). In turn, the only trends that we could not detect when applying the fusion method were for the areas with shoreline changes inside the error margin (18.625 or 5 times the shoreline maximum error), classified as stable. However, these associated errors do not interfere with our results, as our objective is not to detect the absolute changes but rather to detect changes with WRL to classify them as erosional, accretional or dynamic. Based on the r^2 value, we can identify if the changes are significant, allowing to detect those changes that have a clear trend and are not a result of inter-annual or seasonal changes.

Table 3 Shoreline error per image. This value is the sum of the co-register error plus the pixel size which is 2.5 m

Image year	Error co-registering (m)	Pixel error (m)	Total error (m)
2004	1.2	2.5	3.7
2006(a)	1.225	2.5	3.725
2006(b)	0.925	2.5	3.425
2007	1.25	2.5	3.75
2009	1.125	2.5	3.625
2011	0.875	2.5	3.375
2012	1.2	2.5	3.7
2014	0	2.5	2.5

Another consideration is that although higher spatial resolution images would allow minimizing the shoreline error, such as WorldView, Quickbird, or Ikonos (Li et al. 2008; Ashraf et al. 2012; Maglione et al. 2014), the cost associated obtaining this data is often prohibitive in non-developed countries. Alternatively, the use of drones could minimize these costs, but the spatial extension would be reduced, and historical shorelines could not be detected. For this reason, shoreline detection using remote sensing data combined with image fusion is an appealing alternative for studies needed to assess shoreline trends at regional scales and where funding and data availability are limited. Nevertheless, subpixel mapping methods could also be used to enhance shoreline mapping (Pardo-Pascual et al. 2012, 2018; Liu et al. 2016), and future work should explore this technique coupled with pan-sharpening images.

Shoreline Extraction and Change Assessment

The infrared band from Landsat has been used for shoreline assessment (Liu and Jezek 2004; Li and Gong 2016), as well as the SWIR band (Pardo-Pascual et al. 2018). In our case, we

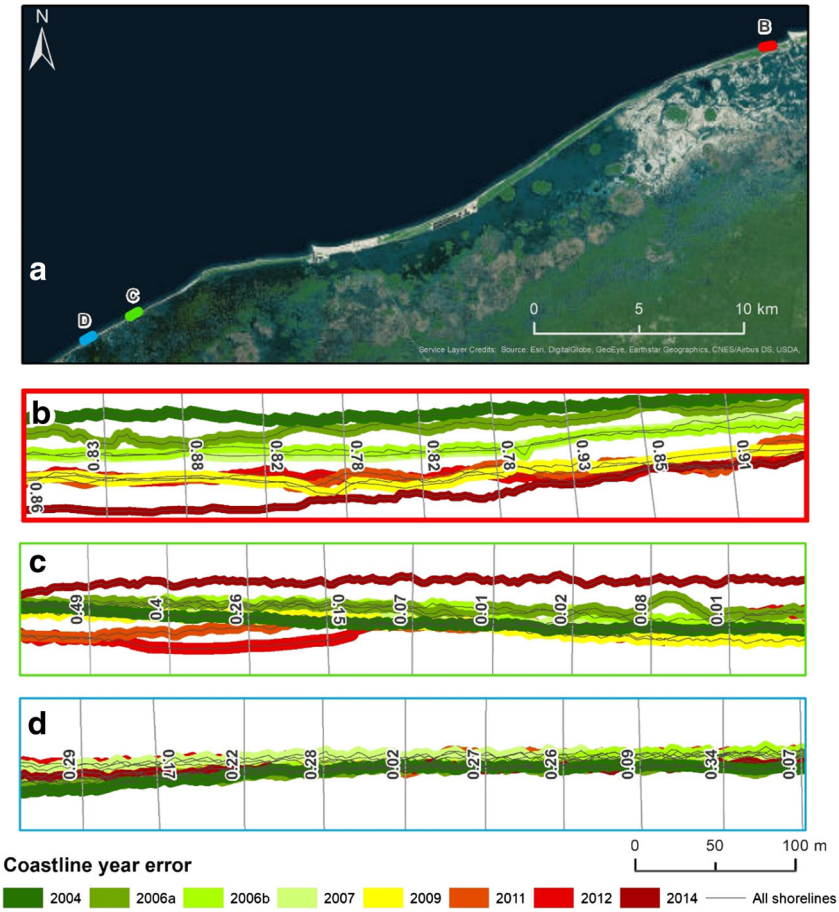

Fig. 7 Examples of transects with different values of r^2 and the shoreline processes they represent. **a** The location of these transects in the study area. **b** Erosion. **c** Dynamic. **d** Stable. The location of these transects in the study area. The width of the shoreline represents its location plus the shoreline error

extracted the shoreline from the green and SWIR bands depending on the tide, as the green band presented an overall higher contrast between the water and the land, while the SWIR band allowed to visualize the shoreline when submerged sandbars were present. As with pan-sharpening, the use of certain bands relies on the sensor and the visual interpretation. Similar to this work, other studies have used DSAS to assess shoreline changes (Alhin and Niemeyer 2009; Kuleli et al. 2011; Aiello et al. 2013; Ford 2013; Ojeda Zújar et al. 2013; Liu et al. 2013; Callaghan et al. 2015; Johnson et al. 2015; Sytnik et al. 2018). These studies did not consider shoreline error and used linear regression or end point rate, and the use of WLR was not necessary since their temporal scales were tens of years. In our case, we used WLR and SCE as the time frame was limited to 10 years, and thus, variations of other time scales (i.e., sea level rise) could not be detected.

Based on the shoreline analysis, we detected stable and dynamic areas as well as areas dominated by erosion or accretionary processes (Fig. 8). With the exception of zone 4, which shows a clear erosional trend, all other zones presented an average WLR suggesting erosion below 1 m/year (Table 4), which confirms the conclusions of Silva-Casarín et al. (2011) stating that the area is undergoing a process of shoreline retreat at a very low rate. Although tidal variations are essential in shoreline mapping, we did not consider tides since we had no in situ water level measurements and considering the microtidal regime the error will be minimal. As such, our goal was to detect shoreline patterns with statistical significance using multi-temporal satellite images and not to determine absolute shoreline changes. While this allows identifying trends, tides should be incorporated when defining precise shoreline positions for design or delineation of areas.

Table 4 Average and standard deviation of WLR and SCE per zone

Zone	Number of transects	WLR	SCE
1	488	− 0.72807 ± 2.471983	24.71264 ± 9.490886
2	119	− 0.02118 ± 2.683399	31.70555 ± 10.35943
3	279	− 0.50086 ± 1.610659	27.51932 ± 12.18205
4	74	− 3.48797 ± 1.040569	36.80419 ± 10.82907

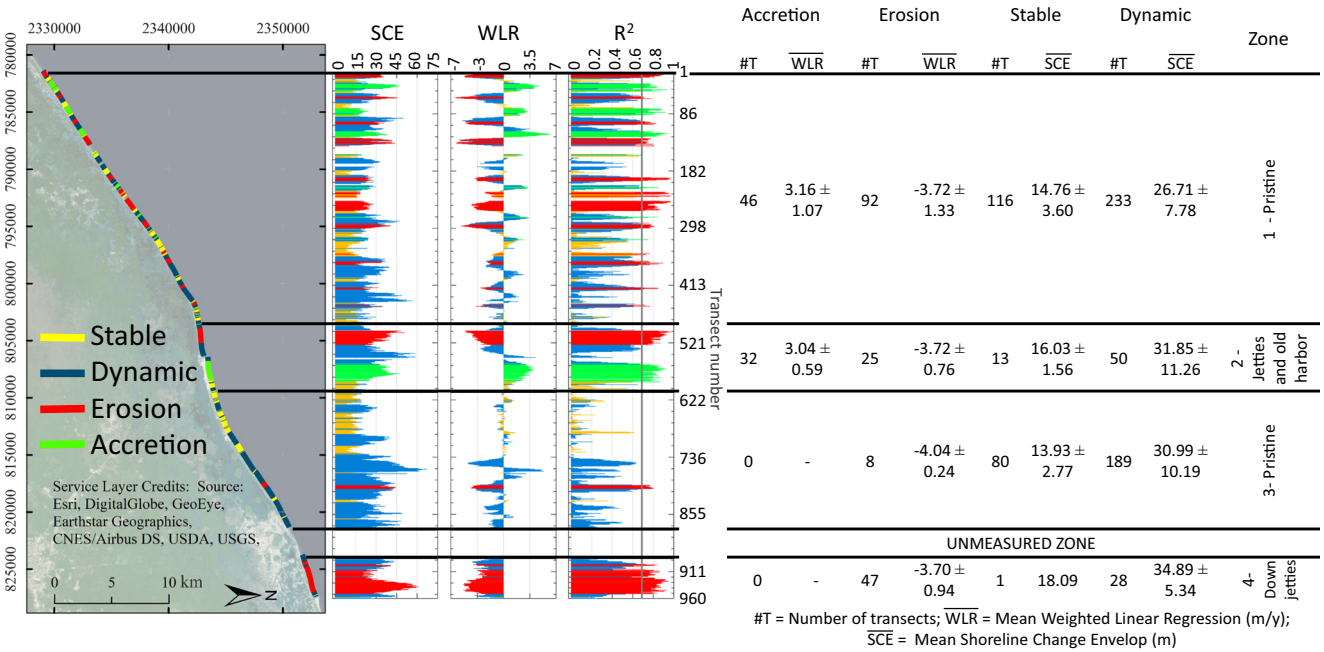

Fig. 8 Classification of the beaches into stable, dynamic, erosion, and accretion, with their respective statistics

The effect of the Sisal and Chuburna harbor jetties induced the most identifiable shoreline changes in the study area, as they interfered with the westward longshore transport that dominates the area (Appendini et al. 2012) and created depositional areas east of the jetties (updrift) and erosional areas to the west/downdrift. Nevertheless, we found that immediately downdrift of the jetties the shorelines were identified as highly dynamic. In these areas, the wave diffraction by the jetties may induce sediment transport inversion (Lira-Pantoja et al. 2012) depending on the wave conditions, leading to either erosion or deposition in the area. Also, the images from January 15, 2006, April 8, 2007, January 4, 2011, and March 3, 2014 correspond to periods of *Norte* events, affecting either the day of the image or the previous 2 days. While normal wave conditions generate a west directed longshore sediment transport, *Norte* events generate waves that inverse the longshore current generating a longshore transport towards the east (Torres-freyermuth et al. 2017). The presence of *Nortes*, therefore, explains deposition patterns to the west of the jetties, where normal conditions will generate erosion, thus leading to the characterization of this shoreline as dynamic. An additional factor to consider is that the updrift areas of the jetties are dredged to prevent shoaling at the harbor entrances and that sediment is moved to the downdrift area (Reyes-Cabañas 2016). This may also induce deposition in an area of expected erosion; unfortunately, there are no records of such interventions. Nevertheless, the clear identification of the erosion and deposition areas show that the method presented can accurately detect shoreline change trends.

Erosion processes were only observed in 20% of the study area. However, not all the erosive shorelines can be attributed to human alteration as less than half of the 221 transects showing erosion corresponded to the regression caused by the jetties in Chuburna (50) and Sisal (33). This indicates that 62% of the shoreline regression occurred in response to natural processes (e.g., grain size and gradients in sediment transport capacity due to natural oscillations in shoreline alignment). Besides the erosion caused by the harbors, the loss of ecosystems is not a natural process in our study area given that 9% of the shoreline shows accretionary processes and 61% show dynamic shorelines in comparison with the only 2% of natural erosion. The erosion–deposition patterns alternating with highly dynamic shorelines occurred mainly in zone 1, which is devoid of coastal infrastructure, and thus, the erosion is a natural process in the area. Based on Appendini et al. (2012), the maximum potential sediment transport capacity in northern Yucatan is attained with a shore normal orientation of 320° N, which corresponds to the orientation at the pristine area. A small change in the shoreline orientation will then create either a decrease or increase in sediment transport, which depending on the orientation shift will create either erosion or deposition area. This indicates that small changes in shoreline orientation may lead to these erosion and deposition patterns, which explain their presence in an area with no human interventions.

The method presented allows classification of erosional, depositional, stable, and dynamic shorelines. These classifications are critical for coastal and shoreline management, as they facilitate planning and delineate development along the coast. For instance, long stretches of stable or depositional areas may indicate suitable places for more permanent structures (provided they will be located in an area where coastal processes will not be affected). In turn, erosional areas may indicate a

high risk for permanent structures. Also, highly dynamic areas could be indicative of shoreline variability, which may be useful for those wanting to plan activities in the area, whether they are seasonal or otherwise.

The case of zone 1 is particularly interesting. While being a pristine and undisturbed area from human interventions, it shows highly dynamic stretches of shoreline intermingled with erosional and depositional areas. Unexpectedly, it shows barely any stable shorelines. This indicates that other processes such as shoreline orientation, sediment transport capacity, and grain size are controlling the shoreline changes. These should be considered if there are any plans for the development of the area. As such, the methodology presented can be used to assess shoreline changes in remote areas with limited data and provide managers with information for future developments or event to determine protected areas.

Conclusions

A first assessment of the shoreline changes in the northwestern coast of Yucatan at a landscape scale was presented. This was achieved by successfully detecting shoreline changes using fused images from SPOT-5 satellite in 10 years. The SPOT-5 images allow for an increased temporal resolution to perform shoreline change analysis, providing better insight into the experienced changes otherwise undetected by using fewer images. Thus, this study demonstrates how significant temporal and spatial resolutions are to study shoreline patterns with satellite images in unexplored and/or inaccessible areas with lack of monitoring.

We found that fused multi-spectral and panchromatic images from SPOT-5 using the HCS algorithm were adequate to detect shoreline changes in 10 years in the northwest of Yucatan at this spatial scale. The method presented is by no means the most adequate method to detect shorelines; while it proved to be the most adequate in our study area, different pan-sharpened method enhancement should be explored for specific study site conditions.

We showed that we can enhance shoreline detection precision with satellite images coupled with image fusion, and that shoreline trends can be detected when analyzing their changes over the years with DSAS by using weighted linear regression (WLR) and r^2, which proved essential to detect shoreline changes in a time scale of few years with multi-temporal resolution. The method presented was shown to be effective for classifying shoreline changes into erosion, accretion, stable, and dynamic segments.

Our results confirm that the shoreline in the northwest of Yucatan is highly dynamic, where there is high variability of erosion and accretion in areas that are affected by structures. The erosion and accretion patterns also occur in pristine areas due to the shoreline having an orientation near the orientation creating maximum potential sediment transport. In such a location, small shifts in wave conditions may lead to positive or negative sediment transport gradients and, in turn, cause dynamic shorelines alternating with erosion/deposition patterns.

The method presented shows its viability to detect shoreline changes in relatively short time frames with low budgets, which are usual constraints in developing countries. The use of this methodology provides a framework to assess shoreline change trends in remote areas and without local measurements, enabling the assessment for development planning and shoreline management.

Future work should include correction of the shorelines by the use of measured coastal profiles and a profound analysis of the climatic seasons in this region. With the advent of more readily available satellite images in the near future, this method can be useful to study shoreline changes in remote areas and under strict budgets. As a final recommendation, we encourage future studies to use WLR as it gives a better interpretation of shoreline changes, as well as considering the shoreline error position for obtaining more accurate results.

Acknowledgments Images are from the Reception Station Mexico New Generation (ERMEX, in Spanish "*Estación de Recepción México Nueva Generación*") in charge of the Ministry of Agriculture, Livestock, Rural Development, Fisheries and Food (SAGARPA, in Spanish "*Secretaría de Agricultura*, *Ganadería*, *Desarrollo Rural*, *Pesca y Alimentación*), and were provided by Rodolfo Rioja Nieto. Water levels for Sisal were provided by José López González. Rodolfo Silva Casarín, Marisa Martinez, and Rosario Landgrave provided helpful critical reviews of this manuscript. We thank Gabriela Medellín Mayoral, Paola Espadas Sánchez, and Daniel Harris for their valuable feedback in the interpretation of our results, as well as Gonzalo Martin for IT support. The authors are thankful to Sevan Houston and Marcel E. Sayre for proofreading the manuscript.

Funding information DAAD and Exceed Swindon funded the Integrating Ecosystems in Coastal Engineering Practice (INECEP) Summer School. This study was funded by project CONACYT 6603. Ana Patricia Ruiz-Beltran was supported by LANRESC through project CONACYT 271544. Christian M. Appendini was supported by DGAPA through PAPIIT project IA100418.

References

Aiello, A., F. Canora, G. Pasquariello, and G. Spilotro. 2013. Shoreline variations and coastal dynamics: a space-time data analysis of the Jonian littoral, Italy. *Estuarine, Coastal and Shelf Science* 129: 124–135. https://doi.org/10.1016/j.ecss.2013.06.012.

Alhin, K.A., and I. Niemeyer. 2009. Coastal monitoring using remote sensing and geoinformation systems: estimation of erosion and accretion rates along Gaza coastline. *International Geoscience and Remote Sensing Symposium (IGARSS)* 4: 29–32. https://doi.org/10.1109/IGARSS.2009.5417605.

Alparone, L., B. Aiazzi, S. Baronti, and A. Garzelli. 2015. *Remote sensing image fusion*. Taylor & Francis Group.

Appendini, C.M., P. Salles, E. Tonatiuh Mendoza, et al. 2012. Longshore sediment transport on the northern coast of the Yucatan Peninsula. *Journal of Coastal Research* 285: 1404–1417. https://doi.org/10.2112/JCOASTRES-D-11-00162.1.

Appendini, C.M., J. Hernández, L. Rafael, et al. 2018. Effect of climate change on wind waves generated by anticyclonic cold front intrusions in the Gulf of Mexico. *Climate Dynamics* 51 (9-10): 3747–3763. https://doi.org/10.1007/s00382-018-4108-4.

Ashraf, S., L. Brabyn, and B.J. Hicks. 2012. Image data fusion for the remote sensing of freshwater environments. *Applied Geography* 32 (2): 619–628. https://doi.org/10.1016/j.apgeog.2011.07.010.

Bai, L., C. Xu, and C. Wang. 2015. A review of fusion methods of multispectral image. *Optik - International Journal for Light and Electron Optics* 126 (24): 4804–4807. https://doi.org/10.1016/j.ijleo.2015.09.201.

Boak, E.H., and I.L. Turner. 2005. Shoreline definition and detection: a review. *Journal of Coastal Research* 214: 688–703. https://doi.org/10.2112/03-0071.1.

Callaghan, K., J. Engelbrecht, and J. Kemp. 2015. The use of Landsat and aerial photography for the assessment of coastal erosion and erosion susceptibility in False Bay, South Africa. *South Africal Journal of Geomatics* 4: 65–79. https://doi.org/10.4314/sajg.v4i2.1.

Castelle, B., B. Guillot, V. Marieu, E. Chaumillon, V. Hanquiez, S. Bujan, and C. Poppeschi. 2018. Spatial and temporal patterns of shoreline change of a 280-km high-energy disrupted sandy coast from 1950 to 2014: SW France. *Estuarine, Coastal and Shelf Science* 200: 212–223. https://doi.org/10.1016/j.ecss.2017.11.005.

Cuevas Jiménez, A., J.I. Euán Ávila, M.M. Villatoro Lacouture, and R. Silva Casarín. 2016. Classification of beach erosion vulnerability on the Yucatan coast. *Coastal Management* 44 (4): 333–349. https://doi.org/10.1080/08920753.2016.1155038.

Cuevas-Jiménez, A., and J. Euán-Ávila. 2009. Morphodynamics of carbonate beaches in the Yucatán Peninsula Morfodinámica. *Ciencias Marinas* 35 (3): 307–320.

Day, J.W., R.R. Christian, D.M. Boesch, A. Yáñez-Arancibia, J. Morris, R.R. Twilley, L. Naylor, L. Schaffner, and C. Stevenson. 2008. Consequences of climate change on the ecogeomorphology of coastal wetlands. *Estuaries and Coasts* 31 (3): 477–491. https://doi.org/10.1007/s12237-008-9047-6.

Defeo, O., A. McLachlan, D.S. Schoeman, T.A. Schlacher, J. Dugan, A. Jones, M. Lastra, and F. Scapini. 2009. Threats to sandy beach ecosystems: a review. *Estuarine, Coastal and Shelf Science* 81 (1): 1–12. https://doi.org/10.1016/j.ecss.2008.09.022.

Di, K., R. Ma, J. Wang, and R. Li. 2003. Coastal mapping and change detection using high-resolution IKONOS satellite imagery. In *Proceedings of the 2003 Annual National Conference on Digital Government Research*, 1–4. Digital Government Society of North America.

Du, P., S. Liu, J. Xia, and Y. Zhao. 2013. Information fusion techniques for change detection from multi-temporal remote sensing images. *Information Fusion* 14 (1): 19–27. https://doi.org/10.1016/j.inffus.2012.05.003.

Emanuel, K.A. 2013. Downscaling CMIP5 climate models shows increased tropical cyclone activity over the 21st century. *Proceedings of the National Academy of Sciences* 110 (30): 12219–12224.

Espadas-Sánchez, P. 2017 Dinámica de la línea de costa en una playa disipativa (Sisal, Yucatán). Master of Engineering Thesis Universidad Nacional Autónoma de México.

Ford, M. 2013. Shoreline changes interpreted from multi-temporal aerial photographs and high resolution satellite images: Wotje Atoll, Marshall Islands. *Remote Sensing of Environment* 135: 130–140. https://doi.org/10.1016/j.rse.2013.03.027.

García-Rubio, G., D. Huntley, and P. Russell. 2015. Evaluating shoreline identification using optical satellite images. *Marine Geology* 359: 96–105. https://doi.org/10.1016/j.margeo.2014.11.002.

Garguet-Duport, B., J. Girel, J. Chassery, and G. Pautou. 1996. The use of multiresolution analysis and wavelets transform for merging SPOT panchromatic and multispectral image data. *Photogrammetric Engineering and Remote Sensing* 62: 1057–1066.

Gens, R. 2010. Remote sensing of coastlines: detection, extraction and monitoring. *International Journal of Remote Sensing* 31 (7): 1819–1836. https://doi.org/10.1080/01431160902926673.

Ghosh, M.K., L. Kumar, and C. Roy. 2015. Monitoring the coastline change of Hatiya Island in Bangladesh using remote sensing techniques. *ISPRS Journal of Photogrammetry and Remote Sensing* 101: 137–144. https://doi.org/10.1016/j.isprsjprs.2014.12.009.

Herrera-Silveira, J.A., C. Enriquez, and I.J. Marin. 2010. Dispersion in the Yucatan coastal zone: implications for red tide events. *Continental Shelf Research* 30 (2): 127–137. https://doi.org/10.1016/j.csr.2009.10.005.

Houser, C., Wernette, P., Rentschlar, E., Jones, H., Hammond, B., & Trimble, S. 2015. Post-storm beach and dune recovery: Implications for barrier island resilience. *Geomorphology* 234:54-63.

Huhdanpaa, H., D.H. Hwang, G.G. Gasparian, M.T. Booker, Y. Cen, A. Lerner, O.B. Boyko, J.L. Go, P.E. Kim, A. Rajamohan, M. Law, and M.S. Shiroishi. 2014. Image coregistration: quantitative processing framework for the assessment of brain lesions. *Journal of Digital Imaging* 27 (3): 369–379. https://doi.org/10.1007/s10278-013-9655-y.

Johnson, J.M., L.J. Moore, K. Ells, A.B. Murray, P.N. Adams, R.A. MacKenzie III, and J.M. Jaeger. 2015. Recent shifts in coastline change and shoreline stabilization linked to storm climate change. *Earth Surface Processes and Landforms* 40 (5): 569–585. https://doi.org/10.1002/esp.3650.

Kang, N.-Y., and J.B. Elsner. 2015. Trade-off between intensity and frequency of global tropical cyclones. *Nature Climate Change* 5 (7): 661–664. https://doi.org/10.1038/nclimate2646.

Kermani, S., M. Boutiba, M. Guendouz, M.S. Guettouche, and D. Khelfani. 2016. Detection and analysis of shoreline changes using geospatial tools and automatic computation: case of jijelian sandy coast (East Algeria). *Ocean and Coastal Management* 132: 46–58. https://doi.org/10.1016/j.ocecoaman.2016.08.010.

Knutson, T.R., J.L. McBride, J. Chan, et al. 2010. Tropical cyclones and climate change. *Nature Geoscience* 3 (3): 157–163. https://doi.org/10.1038/ngeo779.

Kuleli, T., A. Guneroglu, F. Karsli, and M. Dihkan. 2011. Automatic detection of shoreline change on coastal Ramsar wetlands of Turkey. *Ocean Engineering* 38 (10): 1141–1149. https://doi.org/10.1016/j.oceaneng.2011.05.006.

Li, X., and M.C.J. Damen. 2010. Coastline change detection with satellite remote sensing for environmental management of the Pearl River Estuary, China. *Journal of Marine Systems* 82: S54–S61. https://doi.org/10.1016/j.jmarsys.2010.02.005.

Li, W., and P. Gong. 2016. Continuous monitoring of coastline dynamics in western Florida with a 30-year time series of Landsat imagery. *Remote Sensing of Environment* 179: 196–209. https://doi.org/10.1016/j.rse.2016.03.031.

Li, Y., J. Li, and Y. Lu. 2008. A fuzzy segmentation-based approach to extraction of coastlines from Ikonos imagery. *Geomatica* 62: 407–417.

Lin, C., C.-C. Wu, K. Tsogt, Y.C. Ouyang, and C.I. Chang. 2015. Effects of atmospheric correction and pansharpening on LULC classification accuracy using WorldView-2 imagery. *Information Processing in Agriculture* 2 (1): 25–36. https://doi.org/10.1016/j.inpa.2015.01.003.

Lira-Pantoja, M.A., Torres-Freyermuth, A., Appendini, C.M., et al. 2012. Chronic beach erosion induced by coastal structures in Chelem, Yucatán. In: Coastal Engineering Proceedings. pp 1–10.

Liu, H., and K.C. Jezek. 2004. Automated extraction of coastline from satellite imagery by integrating canny edge detection and locally adaptive thresholding methods. *International Journal of Remote Sensing* 25 (5): 937–958. https://doi.org/10.1080/0143116031000139890.

Liu, Y., H. Huang, Z. Qiu, and J. Fan. 2013. Detecting coastline change from satellite images based on beach slope estimation in a tidal flat.

International Journal of Applied Earth Observation and Geoinformation 23: 165–176. https://doi.org/10.1016/j.jag.2012.12.005.

Liu, Q., J. Trinder, and I. Turner. 2016. A comparison of sub-pixel mapping methods for coastal areas. *ISPRS Annals of the Photogrammetry, Remote Sensing and Spatial Information Sciences* 3: 67–74. https://doi.org/10.5194/isprs-annals-III-7-67-2016.

Maglione, P., C. Parente, and A. Vallario. 2014. Coastline extraction using high resolution WorldView-2 satellite imagery. *European Journal of Remote Sensing* 47 (1): 685–699. https://doi.org/10.5721/EuJRS20144739.

Maiti, S., and A.K. Bhattacharya. 2009. Shoreline change analysis and its application to prediction: a remote sensing and statistics based approach. *Marine Geology* 257 (1-4): 11–23. https://doi.org/10.1016/j.margeo.2008.10.006.

Mendoza, E.T., E. Ojeda-Casillas, K.J. Meyer-Arendt, et al. 2014. Assessing coastal vulnerability in Yucatan (Mexico). *Coastal management: changing coast, changing climate, changing minds* 1–9. https://doi.org/10.1680/cm.61149.607.

Neal, T.C., Rankey, E.C., Appendini, C.M. 2016. Hydrodynamic controls on sedimentology and geomorphology: a field and modeling analysis of modern carbonate ramp, Northern Yucatan Shelf, Mexico. In American Association of Petroleum Geologists Annual Conference. Calgary.

Ojeda Zújar, J., M.D.P. Díaz Cuevas, A. Prieto Campos, and J.I. Álvarez Francoso. 2013. Línea de costa y sistemas de información geográfica: modelo de datos para la caracterización y cálculo de indicadores en la costa andaluza. *Investigaciones Geográficas* (60): 37–52. https://doi.org/10.14198/INGEO2013.60.02.

Padwick, C., Deskevich, M., Pacifici, F., Smallwood, S. 2010. WorldView-2 pan-sharpening. In ASPRS 2010. pp 26–30.

Pardo-Pascual, J.E., J. Almonacid-Caballer, L.A. Ruiz, and J. Palomar-Vázquez. 2012. Automatic extraction of shorelines from Landsat TM and ETM+ multi-temporal images with subpixel precision. *Remote Sensing of Environment* 123: 1–11. https://doi.org/10.1016/j.rse.2012.02.024.

Pardo-Pascual, J.E., E. Sánchez-García, J. Almonacid-Caballer, J. Palomar-Vázquez, E. Priego de los Santos, A. Fernández-Sarría, and Á. Balaguer-Beser. 2018. Assessing the accuracy of automatically extracted shorelines on microtidal beaches from Landsat 7, Landsat 8 and Sentinel-2 imagery. *Remote Sensing* 10 (2): 1–20. https://doi.org/10.3390/rs10020326.

Petropoulos, G.P., D.P. Kalivas, H.M. Griffiths, and P.P. Dimou. 2015. Remote sensing and GIS analysis for mapping spatio-temporal changes of erosion and deposition of two Mediterranean river deltas: the case of the Axios and Aliakmonas rivers, Greece. *International Journal of Applied Earth Observation and Geoinformation* 35: 217–228. https://doi.org/10.1016/j.jag.2014.08.004.

Pohl, C., and J.L. Van Genderen. 1998. Review article multisensor image fusion in remote sensing: concepts, methods and applications. *International Journal of Remote Sensing* 19 (5): 823–854. https://doi.org/10.1080/014311698215748.

Pontee, N. 2013. Defining coastal squeeze: a discussion. *Ocean and Coastal Management* 84: 1–4. https://doi.org/10.1016/j.ocecoaman.2013.07.010.

Pradham, P., N.H. Younan, and R.L. King. 2011. Concepts of image fusion in remote sensing applications. In *Image fusion: algorithms and applications*, 500.

Pranzini, E. 2007. Beach variability and shoreline evolution monitoring. In *Beach erosion monitoring*, ed. E. Pranzini and L. Wetzel, 13–14.

Reyes-Cabañas, P.E. 2016. Dimensionamiento de un sistema de bypass de arena en el puerto de Sisal, Yucatán. Master of Engineering Thesis. Universidad Nacional Autónoma de México.

Ruiz-Martínez, G., I. Mariño-Tapia, E.G. Mendoza Baldwin, et al. 2015. Identifying coastal defence schemes through morphodynamic numerical simulations along the northern coast of Yucatan, Mexico. *Journal of Coastal Research* 651–670. https://doi.org/10.2112/JCOASTRES-D-15-00009.1.

Sagar, S., D. Roberts, B. Bala, and L. Lymburner. 2017. Extracting the intertidal extent and topography of the Australian coastline from a 28year time series of Landsat observations. *Remote Sensing of Environment* 195: 153–169. https://doi.org/10.1016/j.rse.2017.04.009.

Silva-Casarín, R., Lacouture, M., Durón, F., et al. 2011. Caracterización de la zona costera y planteamiento de elementos técnicos para la elaboración de criterios de regulación y manejo sustentable. Report.

Silva-Casarín, R., M.L. Martínez, P.A. Hesp, et al. 2014. Present and future challenges of coastal erosion in Latin America. *Journal of Coastal Research* 71: 1–16. https://doi.org/10.2112/SI71-001.1.

Sytnik, O., L. Del Río, N. Greggio, and J. Bonetti. 2018. Historical shoreline trend analysis and drivers of coastal change along the Ravenna coast, NE Adriatic. *Environmental Earth Sciences* 77 (23): 779. https://doi.org/10.1007/s12665-018-7963-8.

Syvitski, J.P.M., and J.D. Milliman. 2017. Geology, geography, and humans battle for dominance over the delivery of fluvial sediment to the coastal ocean. *The Journal of Geology* 115: 1–19.

Thieler RE, Himmelstoss EA, Zichichi JL, Ergul A (2009) The digital shoreline analysis system (DSAS) version 4.0 - an ArcGIS extension for calculating shoreline change.

Torres-Freyermuth, A., J.A. Puleo, N. Dicosmo, et al. 2017. Nearshore circulation on a sea breeze dominated beach during intense wind events. *Continental Shelf Research* 151: 40–52. https://doi.org/10.1016/j.csr.2017.10.008.

Vijayaraj, V. 2004. A quantitative analysis of pansharpened images. Master of science thesis. Mississippi State University.

Wang, X., Y. Liu, F. Ling, and S. Xu. 2018. Fine spatial resolution coastline extraction from Landsat-8 OLI imagery by integrating downscaling and pansharpening approaches. *Remote Sensing Letters* 9 (4): 314–323. https://doi.org/10.1080/2150704X.2017.1420928.

Yang, X. 2009. *Remote sensing and geospatial technologies for coastal ecosystem assessment*. Berlin: Springer.

Zulkifle, F.A., R. Hassan, S. Kasim, and R.M. Othman. 2017. A review on shoreline detection framework using remote sensing satellite image. *International Journal of Innovative Computing Journal* 7: 40–51.